

Sensing Climate Change Using the Global Positioning System

LESTER L. YUAN,¹ RICHARD A. ANTHES,² RANDOLPH H. WARE,³ CHRISTIAN ROCKEN,³
WILLIAM D. BONNER,² MICHAEL G. BEVIS⁴, and STEVEN BUSINGER⁴

Using simulated atmospheric data from the National Center for Atmospheric Research (NCAR) community climate model (CCM), we test the hypothesis that the global positioning system (GPS) can be used to detect global and regional climate change. We examine how the fundamental GPS variables (wet and total delays and vertical profiles of refractivity) as well as precipitable water as estimated by ground-based GPS receivers would change in a climate with 2 times the present concentration of carbon dioxide (CO₂). Because of the higher water vapor content in the doubled CO₂ simulation the wet delay and the precipitable water show a significant increase in the tropics and middle latitudes. Refractivity also shows an increase in the lower troposphere. We also simulate the changes in the GPS signal delay in a doubled CO₂ climate as would be measured by a radio occultation technique using low Earth-orbiting (LEO) satellites equipped with GPS receivers. Increases in temperature and water vapor in the lower troposphere of the model atmosphere produce opposite effects on the occultation delay. Increased temperature tends to decrease the delay, while increased water vapor increases the delay. Amplified by the long "lever arms" of the LEO-atmosphere-GPS link, a strong "greenhouse warming" signal is simulated, with increases in occultation delay of nearly 100 m using the globally averaged data. This increase indicates that globally the effect of increased water vapor dominates. However, significant regional differences are present in the occultation delay response. In the tropics, where the temperature increase is smallest and the water vapor increases are largest, increases in delay of about 300 m are simulated. In contrast, in the polar regions where the increased temperatures are greatest and the increases in water vapor are smallest, the temperature effect dominates and a decrease in occultation delay of nearly 70 m is simulated. When compared to expected errors in measuring the occultation delay of about 1 m, these results indicate that monitoring trends in occultation delays would be a practical way to detect global and regional climate change.

INTRODUCTION

This paper describes model simulations of a new approach to measuring atmospheric water vapor in the troposphere and temperature in the upper atmosphere for use in operational weather forecasting and weather and climate research. The approach involves using the global positioning system (GPS). GPS was originally designed as a highly accurate navigational system but has become a widely used tool by geodesists, geophysicists, and surveyors because of its capability for very precise positioning. In GPS geodesy the distances between GPS satellites and GPS receivers are determined by measuring the time of propagation of radio signals from satellites to receivers. This time is affected by the temperature and the water vapor content of the atmosphere along the path of propagation. For the purposes of geodesy the effects of the atmosphere must be removed to the extent possible. However, this "noise" to the geodesist is a "signal" to the atmospheric scientist [Hardy *et al.*, 1992; Bevis *et al.*, 1992, 1993].

Using GPS, researchers could measure vertical profiles of refractivity, a characteristic of the atmosphere depending upon the local pressure, temperature, and moisture. From this refractivity information it is possible to extract temperature or moisture data which could be incorporated into regional or global numerical weather prediction (NWP) models, ultimately improving forecasts. Another promising application of GPS data is the detection of global and regional climate change by the

monitoring of global data sets of temperature and moisture. More importantly, though, the raw GPS signal delay data themselves could potentially provide a sensitive indicator of climate change.

Bevis *et al.* [1992, 1993] discussed the idea of GPS meteorology and proposed a method of using GPS to measure atmospheric water vapor content. They showed that the integrated water vapor (IWV) overlying a ground-based GPS receiver can be computed from the measured "zenith wet delay" with a total error (random plus systematic) of approximately 5%. Extending these ideas, we have simulated the measurement of various GPS variables using data files from the NCAR community climate model (CCM). We have also examined the sensitivity of these variables to global warming and climate change as simulated by the CCM and in so doing have determined characteristic changes which would be indicative of global warming.

2. GLOBAL POSITIONING SYSTEM (GPS) METEOROLOGY: BACKGROUND

2. GPS Variables

The fundamental variable measured by GPS techniques is the signal delay. As the GPS radio signal travels from satellite to receiver, it is affected by the atmosphere in two distinct ways. First, the signal bends in response to gradients in the index of refraction of the atmosphere, traveling a curved path in contrast with the straight-line path the signal would travel in a region of constant refractivity. The difference between the lengths of these two paths is known as the geometrical delay. Second, the waves travel slower in a region of finite density than they would in a vacuum. The increase in the time required to cover a given distance can also be expressed in terms of excess path length, yielding the optical delay. The total delay, then, is the sum of these two components and can be written in the following manner:

$$\Delta L = \int_L n(s) ds - G \quad (1)$$

where $n(s)$ is the refractive index as a function of position s along the curved path L , and G is the geometrical straight-line path

¹Stanford University, Stanford, California.

²University Corporation for Atmospheric Research (UCAR), Boulder, Colorado.

³University Navstar Consortium (UNAVCO), Boulder, Colorado.

⁴Department of Marine, Earth and Atmospheric Sciences, North Carolina State University, Raleigh, North Carolina.

length through the atmosphere. This equation can be rewritten in term of atmospheric refractivity, N , which is defined by

$$N = 10^6 (n - 1) \quad (2)$$

giving

$$\Delta L = 10^{-6} [Nds + \{S-G\}] \quad (3)$$

where S is the curved path length along L . In this form, the first term of the equation corresponds to optical delay, while the second term corresponds to geometrical delay. The atmospheric refractivity is a function of the local density, or equivalently, the local pressure, temperature, and water vapor content. The following relation

$$N = 77.6 \frac{P}{T} + 3.73 \times 10^5 \frac{P_v}{T^2} \quad (4)$$

suggested by *Smith and Weintraub* [1953], provides an accuracy of approximately 0.5%, where P is the total atmospheric pressure in millibars (mbar), T is the absolute atmospheric temperature in Kelvins, and P_v is the partial pressure of water vapor, also in millibars.

2.1.1.1. *Temperature and water vapor profiles from GPS data.* From (4) one can see that if the signal delay is known and an independent source of temperature profile information is available, then computation of water vapor profiles becomes possible. Similarly, independent water vapor information would allow the computation of vertical temperature profiles. We can estimate the minimum error of these calculations if we assume, for the purpose of this calculation, that we know the uncertainty associated with the independent temperature or water vapor data and if we assume that the refractivity profile is exact.

Differentiating and rearranging the equation for refractivity (4) at a constant pressure gives

$$2TNdT + T^2 dN = aPdT + c dP_v \quad (5)$$

with the constant $a = 77.6$ K/mbar and $c = 3.73 \times 10^5$ K²/mbar. Assuming that the errors are small and can be represented approximately by the differentials in (5), then if N is exact ($dN = 0$), we arrive at an expression relating the error of the temperature to the error of the partial pressure of water vapor,

$$dT = \frac{dP_v}{aP + \frac{2cP_v}{T}} \quad (6)$$

Using values appropriate for low to midlevels in a tropical atmosphere ($P = 700$ mbar, $P_v = 6$ mbar, and $T = 283$ K), the relationship between the temperature and the water vapor errors is

$$dT \approx (5.3 \frac{K}{mbar}) dP_v \quad (7)$$

Under these conditions, if the water vapor pressure is known to an accuracy of 1 mbar, the error in the computed temperature would be approximately 5.3 K, which is too large to be useful in NWP or in climate studies. However, if instead, temperature profiles are known to an accuracy of approximately 1.5 K, which is a typical operational analysis or short-range (6-12 hours) forecast error, then water vapor could be calculated from refractivity information to an accuracy of about 0.29 mbar, an accuracy that could be useful for both NWP and climate studies. Since current

models predict temperature more accurately than they predict water vapor, one can envision coupling refractivity profile information with short-term model temperature forecasts to obtain usefully accurate vertical distributions of water vapor. At high altitudes or high latitudes where the water vapor pressure is low and $dP_v \approx 0$, or over land areas where the vertical profiles of water vapor may be well known, measurements of signal delay may provide useful estimates of temperature instead.

2.1.2. *Estimating precipitable water from GPS data.* Estimating precipitable water from GPS delay measurements makes use of the unique, dipole nature of atmospheric water vapor. The neutral atmosphere is composed of a mixture of gases, including water vapor, and each component contributes separately to the total refractivity. Water vapor, in addition, also contributes a significant dipole moment effect. As summarized by *Bevis et al.* [1992] it is possible to separate the total delay into two components, a hydrostatic, nondipole portion which depends only upon surface pressure and a wet, dipole portion which depends upon the vertical distribution of water vapor.

The hydrostatic delay in the zenith direction (ZHD) can be expressed in terms of surface pressure by

$$\Delta L_h^0 = ZHD = (2.779 \pm 0.0024) \frac{P_s}{f(\lambda, H)} \quad (8)$$

where P_s is the total surface pressure in millibars and $f(\lambda, H)$ is a factor close to unity accounting for the variation in gravitational acceleration with latitude and height.

The second component of the delay, the zenith wet delay (ZWD) is given by

$$\Delta L_w^0 = ZWD = 10^{-6} \left(k_2' \int \frac{P_v}{T} dz + k_3 \int \frac{P_v}{T^2} dz \right)$$

where $k_2' = (17 \pm 10) \frac{K}{mbar}$ (9)

$$\text{and } k_3 = (3.776 \pm 0.03) 10^5 \frac{K^2}{mbar}$$

An approximate value for the integrated water vapor (IWV) can be calculated from ZWD, with the following relation,

$$IWV = \int \rho_v dz \approx \kappa(ZWD) \quad (10)$$

where the constant κ is given by

$$\frac{1}{\kappa} = 10^{-6} \left(\frac{k_3}{T_m} + k_2' \right) R_v \quad (11)$$

R_v is the specific gas constant for water vapor and the integrated mean temperature, T_m , is given by

$$T_m = \frac{\int \frac{P_v}{T} dz}{\int \frac{P_v}{T^2} dz} \quad (12)$$

Atmospheric water vapor content can also be stated in terms of precipitable water (PW), which is simply the IWV divided by the density of water.

From (10) - (12), if the vertical profiles of temperature and water vapor partial pressure are known exactly, then the calculation of T_m and IWV would also be exact. However, such data are rarely available, so T_m must be estimated. *Bevis et al.* [1992, 1993] suggest that one could compute T_m from profile data provided by short-range forecasts from operational meteorological models. In the absence of such forecasts, one can also relate T_m to local surface temperature by statistical analysis of many radiosonde profiles. Using this approach, *Bevis et al.*

[1992] find that an analysis of 8718 radiosonde profiles spanning a 2-year interval from sites in the United States with a latitude range of 27° N to 65° N yields a linear regression

$$T_m = 70.2 + 0.72T_g \quad (13)$$

with an rms deviation of 4.7 K. Thus if ZWD and surface temperature are known without error, one can compute PW with an average error of less than 4%. This error represents an upper bound; recent results indicate that T_m can be predicted using 12-hour operational forecasts with an rms error of 2.4 K [Bevis et al., 1993].

2.2. GPS Sensing Techniques

There are two primary methods by which GPS can be used for sensing properties of the Earth's atmosphere. The first technique utilizes stationary ground-based receivers. This technique, originally developed for high-precision geodesy can determine relative positions on the Earth with an accuracy of the order of one millimeter. This is achieved through accurate modeling of all GPS signal delays, including the delay caused by the Earth's atmosphere. Geodesists and geophysicists have developed techniques to determine this delay from the GPS data simultaneously with other parameters such as GPS satellite orbits and station coordinates. Thus stationary, ground-based receivers provide integrated information about the atmosphere overlying the receiver. Total delays, as determined with GPS, are usually expressed in terms of paths in the zenith direction and then converted via various mapping functions to account for satellite positions which are not directly overhead.

For a given GPS measurement, ZHD can be calculated from the local surface pressure and subtracted from the total delay. Typically in GPS data processing the ZWD can be estimated by least squares or stochastic techniques as a correction to the a priori value of the ZHD. It has been shown that stochastic methods recover ZWD with a long-term bias of approximately 10 mm and random noise of also approximately 10 mm [Herring et al., 1990; Elgered et al., 1990].

A second method of obtaining GPS soundings of the atmosphere is by means of occultation readings from the GPS transmitter to a low Earth orbit (LEO) satellite (Figure 1). Occultation techniques were originally developed as a means by which probes could measure atmospheric properties of other planets in the solar system. To extract atmospheric information from the LEO data, first the orbit of the LEO must be determined. This task can be achieved using GPS data from the LEO. Once the LEO - GPS configuration is known accurately, the GPS measurements of an occulting LEO can be interpreted in terms of atmospheric delay. This delay is, in part, caused by the neutral atmosphere and in part by the ionosphere. For climatological studies, as described in this paper, the ionospheric delay must be corrected. The effect of the ionosphere on the GPS signal is larger and far more variable than the effect of the neutral atmosphere. We can, however, correct for the ionospheric effect by exploiting the dual frequency signal transmitted by the GPS satellites. The ionosphere affects each GPS frequency differently. This dispersive effect is well known and describes the ionospheric delay as proportional to the inverse of the squared carrier frequency. Thus the travel time difference between the two GPS signals and this known dispersion relation are commonly used to correct for the ionosphere [Spilker, 1980]. This simple correction technique assumes that both GPS frequencies travel along the same path from the GPS satellite to the LEO. While sufficient for ground-based GPS, this assumption will generally not be true for LEO observations where the two frequencies travel along paths, separated by several 100 m. This path separation could lead to ionospheric correction errors of 1 m or more. A recent paper by Brunner and Gu [1991] describes how path separation effects

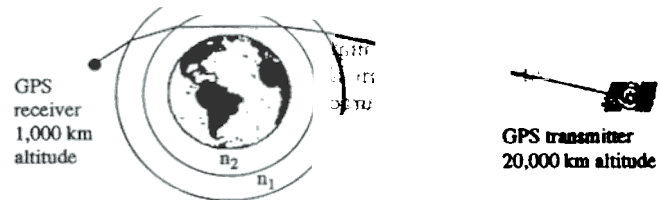


Fig. 1. Global positioning system (GPS) occultation geometry used for path delay calculations. Ray paths through two (exaggerated) atmospheric layers with indices of refraction n_1 and n_2 are shown. The community climate model (CCM) actually comprises nine layers.

may be compensated. GPS occultation work will have to implement corrections similar to those suggested by Brunner and Gu in order to achieve the highest accuracy possible.

3. CLIMATE MODEL

The simulated atmospheric data used for this study were selected from output files from a numerical experiment performed by Washington and Meehl [1984] in which the NCAR CCM was coupled with a simple mixed layer ocean model. The model was run to equilibrium for $1\times\text{CO}_2$ and $2\times\text{CO}_2$ cases and the resulting data fields collected and compared. The data consisted of daily output for the months of January and July. For the purposes of this study, we assumed that the model produced a realistic simulation of the present climate and the changes that would occur as a result of doubling of CO_2 . However, because of the size and complexity of the coupled atmosphere-ocean system, all climate model simulations contain significant uncertainties. Comparing these model data with a later simulation with different physical parameterizations, Meehl and Washington [1990] find that the qualitative changes that occur due to the doubled CO_2 are consistent with the simulation used in this study. Thus although the simulated changes that occur in the GPS variables due to global warming as computed from these CCM data contain uncertainties, the general magnitude and trend of the changes are probably reasonable.

4. MODEL SIMULATIONS OF PW MEASUREMENTS

Accurate information regarding the amount and horizontal distribution of precipitable water leads to significant improvements in NWP forecasts [Kuo et al., 1993]. As mentioned before, with reasonable estimates of the integrated mean temperature (T_m), PW can be calculated with high accuracy from measured zenith wet delays. We tested this assertion using model output for several different days and locations. At each model grid point, ZWD and PW were computed "exactly" by numerical integration of the vertical profiles of water vapor and temperature. We then used (10) to approximate precipitable water from the wet delay, using three different methods to estimate T_m . The simplest method was to assume an empirically derived constant value for T_m of 264.5 K. For the second method we computed T_m from model variables 24 hours earlier than the specified time. This method is equivalent to a 24-hour persistence forecast; use of a 24-hour forecast from an operational model would produce more accurate results. The final method was to apply the empirically derived linear regression given by (13), i.e., computing T_m from the local surface temperature. Approximate PW values were then compared with exact values.

Overall, it appears that ZWD measurements are an excellent means of obtaining precipitable water data. In a tropical region in which day-to-day variations of PW can be as large as 30 mm, even using a constant T_m reproduces the large synoptic fluctuations, while the two more sophisticated schemes predict

PW with excellent accuracy (Figure 2). For regions and seasons in which the atmospheric water vapor content is lower, the accuracy of all three methods improves. For example, for January in a region of the midwestern United States all three methods reproduce PW with good accuracy (Figure 3). The relative error of each prediction method was also computed for each region (Figure 4). As expected, the constant T_m method produces the highest errors, ranging from 5% to 12%. However, the magnitudes of the errors produced by the empirical correlation and the 24-hour persistence forecast are nearly identical, ranging from 1% to 4% (Figure 4). Thus we have confirmed the *Bevis et al.* [1992] estimate of a maximum error of 5% for the inversion from signal delay to PW.

5. DETECTION OF CLIMATE CHANGE

The coupled atmosphere-ocean climate model used in this study indicates changes in global temperature and pressure distributions and in atmospheric water vapor content when atmospheric CO_2 content is doubled. Table 1 gives the values of height, pressure, refractivity, virtual temperature, temperature and water vapor mixing ratio at the nine model sigma (equal to P/P_s) levels in the control (present) climate, and the climate with the doubled CO_2 . Figure 5a shows the vertical profiles of globally averaged temperature for July for the control climate and the climate with doubled CO_2 . The temperature difference between

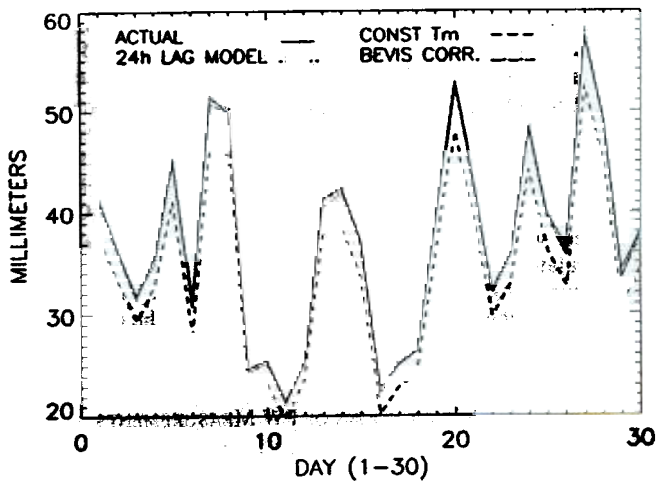


Fig. 2. Comparison of precipitable water prediction methods for January, tropical grid point.

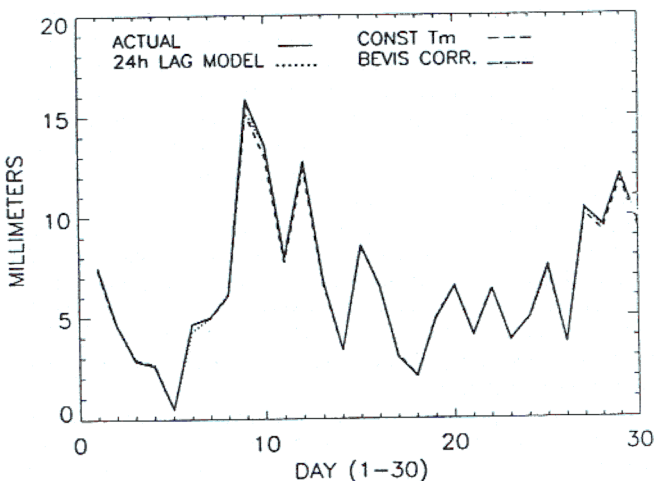


Fig. 3. Comparison of precipitable water prediction methods for January, central U.S. grid point.

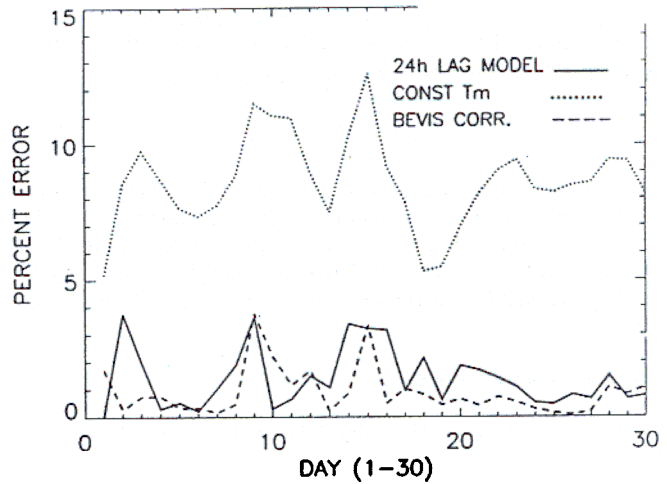


Fig. 4. Comparison of relative accuracy of three precipitable water prediction methods. Data correspond to July at a point located in the central United States.

the two profiles is plotted in Figure 5b. In the lower troposphere the model predicts an increase in globally averaged temperature of approximately 4 K, while in the stratosphere a cooling of as much as 5 K is predicted. A greater surface temperature change occurs in the polar regions of the Earth, with temperature increases of approximately 8 K predicted by the model (Figure 6).

Elevated temperatures in the lower atmosphere lead to increased evaporation which, in turn, produces a higher atmospheric water vapor content. This effect can be seen in Table 1 and Figures 7 and 8, where precipitable water shows an increase in the doubled CO_2 climate. In the tropical zones, precipitable water increases by as much as 7 mm. Also, in a northern hemisphere summer, a notable increase occurs in the zone centered around $50^{\circ}N$.

TABLE 1. Globally Averaged Variables in Control (Present) Climate Simulation and Simulation With Doubled CO_2

sigma	p, mbar	z, km	N	T_v , K	T, K	q, g/kg
<i>Control, $P_s = 96870.4$ Pa</i>						
0.991	960.0	0.46	316.6	283.9	282.5	7.77
0.926	897.0	1.02	291.7	280.2	279.0	6.45
0.811	785.6	2.10	241.8	274.9	274.4	3.27
0.664	643.2	3.69	197.8	268.0	267.6	2.19
0.500	484.4	5.89	152.6	252.9	252.8	0.91
0.336	325.5	8.74	108.0	235.4	235.4	0.21
0.189	183.1	12.72	67.4	210.8	210.8	0.01
0.074	71.7	19.01	27.5	202.7	202.7	0.00
0.009	8.7	23.93	3.0	228.1	228.1	0.00
<i>$2 \times CO_2$ $P_s = 96963.3$ Pa</i>						
0.991	960.9	0.46	323.2	288.1	286.4	9.40
0.926	897.9	1.03	296.7	284.3	282.9	7.86
0.811	786.4	2.12	243.7	278.5	277.8	4.07
0.664	643.8	3.73	198.5	271.1	270.6	2.74
0.500	484.8	5.96	151.9	256.2	256.0	1.18
0.336	325.8	8.85	106.9	238.6	238.5	0.29
0.189	183.3	12.87	67.1	212.2	212.2	0.02
0.074	71.8	19.16	27.6	202.5	202.5	0.00
0.009	8.7	24.07	3.1	222.9	222.9	0.00

In this table, sigma is the vertical coordinate of the model and equal to P/P_s , where P is pressure and P_s is surface pressure, z is the height above sea level, N is refractivity, T_v is virtual temperature, T is temperature, and q is the water vapor mixing ratio.

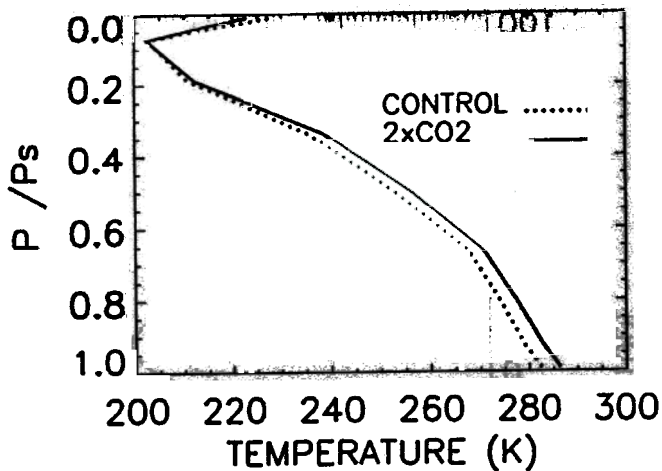


Fig. 5a. Vertical temperature profiles for control climate and 2xCO₂ simulations, July global average.

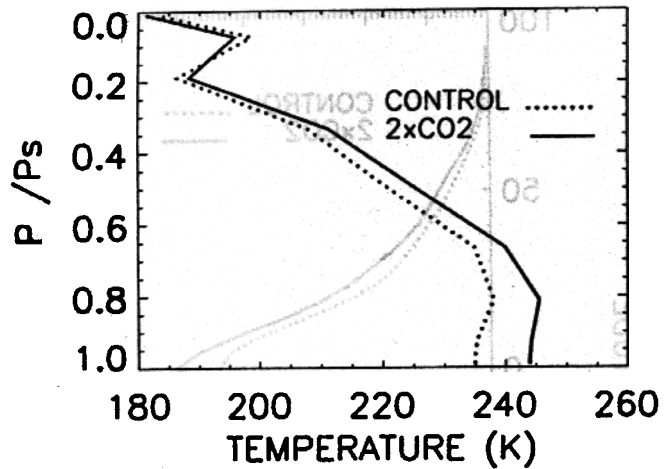


Fig. 6a. Vertical temperature profiles for control climate and 2xCO₂ simulations averaged over south polar region (90°S - 78°S) for July.

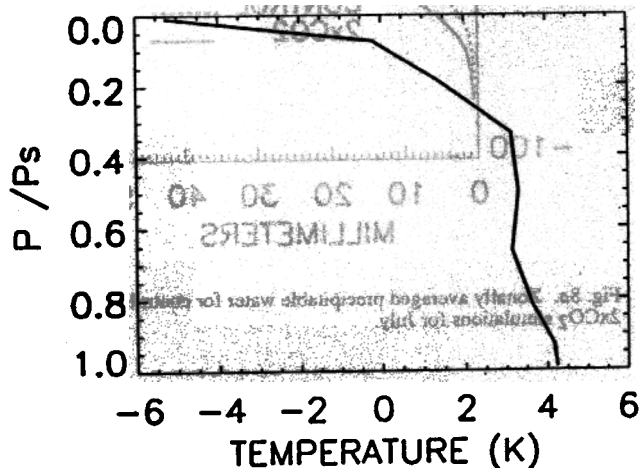


Fig. 5b. Vertical profile of temperature difference in Figure 5a caused by doubled CO₂.

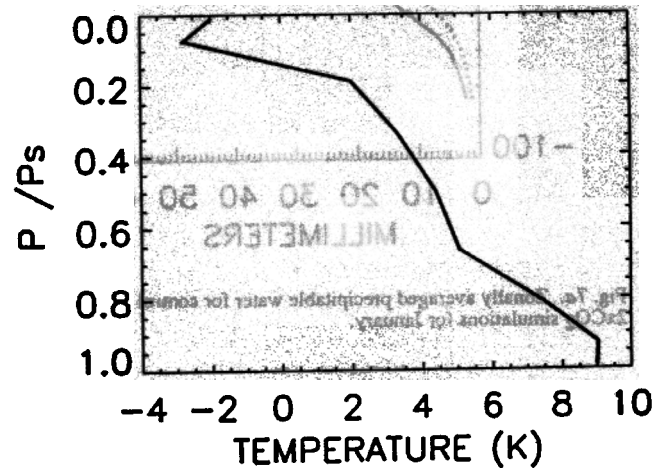


Fig. 6b. Vertical profile of temperature difference in Figure 6a caused by doubled CO₂.

Given that the aforementioned changes occur in the model temperature and water vapor due to increased CO₂ levels, several GPS variables show promise as sensitive indicators of global warming. Because of the distinct increase in precipitable water, monitoring wet delays seems to be an obvious method of detecting global warming. Other fundamental GPS observables, such as refractivity profiles and wet and total delays, might also provide sensitive indicators. In order to fully explore the various avenues of detection available we have examined the sensitivity of all three of these variables to the effects of global warming.

5.1. Zenith Wet Delay

An increase in water vapor due to global warming will produce a concomitant change in ZWD measurements from ground-based receivers. In order to model this effect, ZWD and ZHD values were calculated and averaged zonally over the Earth. The changes that occurred due to the doubled CO₂ were then computed. Not surprisingly, since ZWD is nearly directly proportional to PW, it behaves in a similar fashion to precipitable water as global warming occurs (Figures 9-10). The maximum ZWD increase due to the doubled CO₂ atmosphere is approximately 40 mm. Since ZWD can typically be extracted from the total delay signal with a long-term bias of 10 mm [Bevis *et al.*, 1992], the warming signal is nearly 4 times the size of the average error. Although, this signal to noise ratio is rather small,

the accuracy of GPS measurements and inversion techniques continue to improve and the ratio will increase with time.

5.2. Refractivity

The fundamental variable that can be derived from GPS data, integrated refractivity along the signal path, could also be monitored for global changes. Refractivity varies directly with total pressure and water vapor pressure, while it varies inversely with temperature (equation 4). Thus the lower tropospheric warming predicted by the climate models would tend to decrease refractivity. However, because of the warming, the atmosphere would expand, and at a given height, total pressure would increase, causing a positive change in refractivity. Also, with the warming, the quantity of water vapor in the air increases, again contributing to an increase in refractivity. Thus the increase of temperature and the increase of water vapor produce opposing effects upon refractivity, making the relationship between refractivity and global change quite complex. To simulate the changes that would occur in a doubled CO₂ world, atmospheric refractivity (N) was calculated for all model grid points. Then, appropriate temporal and spatial averages were computed and the differences between vertical profiles in the control and 2xCO₂ simulations compared.

The climate model uses a terrain following vertical coordinate system based upon the sigma variable, defined as local pressure P

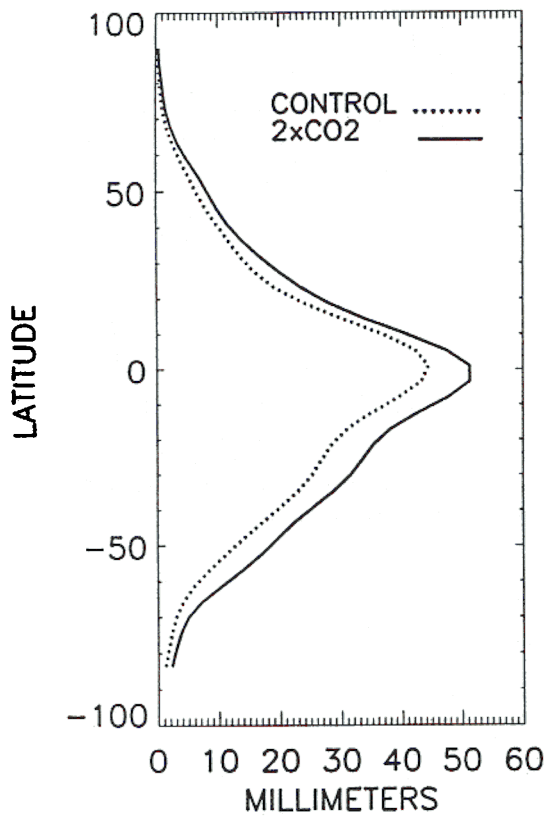


Fig. 7a. Zonally averaged precipitable water for control climate and 2xCO₂ simulations for January.

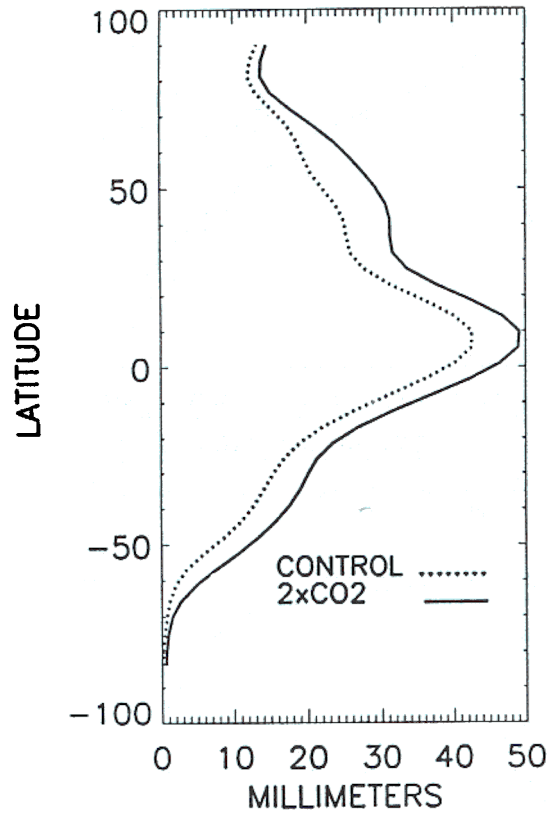


Fig. 8a. Zonally averaged precipitable water for control climate and 2xCO₂ simulations for July.

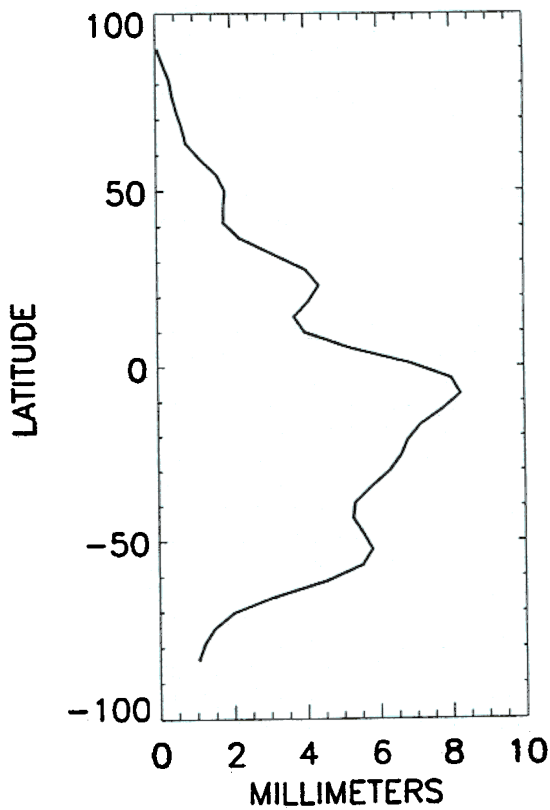


Fig. 7b. Differences in Figure 7a due to doubled CO₂.

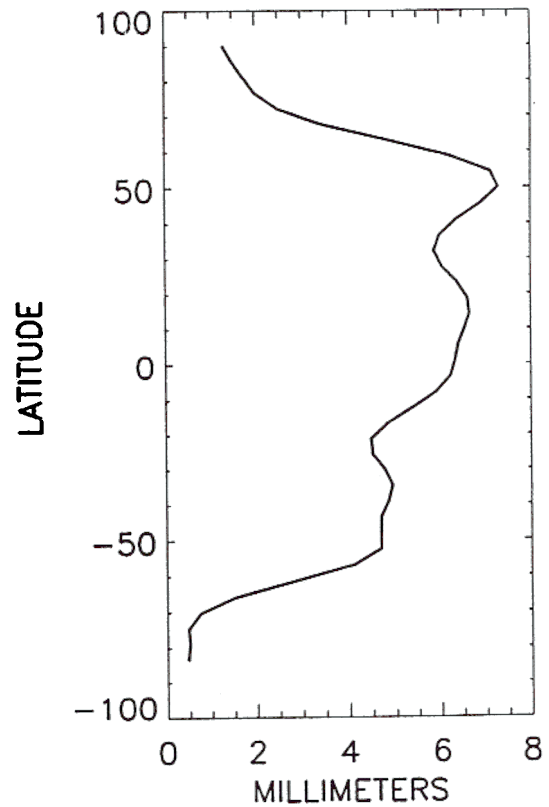


Fig. 8b. Differences in Figure 8a due to doubled CO₂.

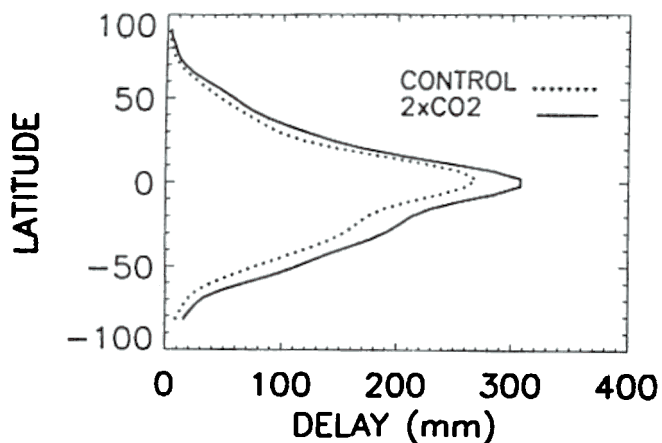


Fig. 9a. Zonally averaged zenith wet delays for control climate and $2\times\text{CO}_2$ simulations for January.

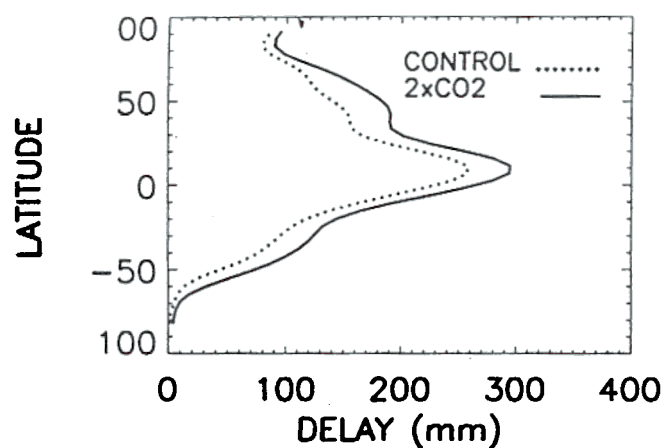


Fig. 10a. Zonally averaged zenith wet delays for control climate and $2\times\text{CO}_2$ simulations for July.

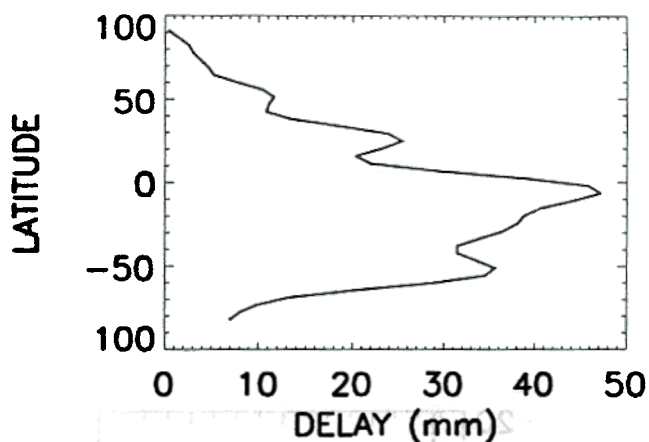


Fig. 9b. Differences in Figure 9a due to doubled CO_2 .

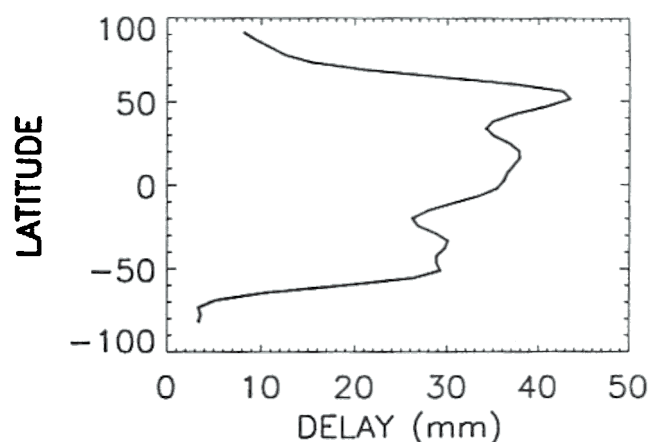


Fig. 10b. Differences in Figure 10a due to doubled CO_2 .

divided by local surface pressure P_s . Initially, we plotted refractivity profiles in terms of sigma. As can be seen in the globally averaged profile for July (Figure 11), the increase in water vapor content of the lower troposphere creates a strong positive change in refractivity due to global warming. As the height increases, though, the water vapor effect decreases, and the effect of elevated temperatures creates a negative signal. For GPS purposes though, vertical profiles plotted in terms of the height above the Earth's surface (z) are more meaningful. In transferring from the sigma to the z coordinate system, an interesting change takes place in the refractivity signal. The strong positive signal in the lower troposphere still exists, but in the upper troposphere the negative signal becomes slightly positive (Figure 12). This phenomenon can be explained in light of the fact that in a warmer climate the atmosphere expands upward. So, for a given height above the surface, total pressure increases (Table 1), which exerts a positive influence upon refractivity, evidently dominating the negative change caused by the elevated temperature.

5.3. Occultation Path Delays

Because of the possibility of obtaining a large number of atmospheric soundings with high temporal and spatial densities, GPS occultation data could prove to be an excellent means of detecting global change. The current limitation to this technique appears to be the increased uncertainty of measurements as the GPS radio waves approach the surface of the Earth. In this region, multipath effects and a strong water vapor signal would serve to increase potential errors. However, in the upper troposphere and

lower stratosphere, GPS occultation data are extremely accurate, with delay errors of the order of 1 cm. At these altitudes the ionospheric error will dominate and ionospheric techniques that are more sophisticated than the standard dual frequency correction described earlier will be required. As the occultation ray passes closer to the Earth's surface, these errors are estimated to increase by an order of magnitude, up to 10–100 cm [Yunck and Melbourne, 1989].

The GPS occultation technique provides values of the signal delay as it travels between the GPS transmitter and the LEO satellite. In order to simulate this effect we implemented a simple ray-tracing algorithm which computes the curved path followed by the GPS signal as it passes through the changing refractivities of the atmosphere. The process is illustrated schematically in Figure 1 for a two-layer model atmosphere (in actuality, the CCM contains nine layers, as indicated in Table 1). Several assumptions were employed to simplify the ray-tracing computation. Ionospheric effects are neglected because the CCM contains only the troposphere and the stratosphere. In the vertical direction the atmosphere was assumed to be composed of layers of constant refractivity, while in the horizontal directions, refractivities were assumed to be homogeneous. Thus the signal follows a straight path through any given layer of the atmosphere and changes directions only at layer interfaces. The bending occurring at each interface is computed by applying Snell's law written for spherical coordinates and using refractivities interpolated from CCM model data at appropriate heights. Each ray trace is computed incrementally by advancing along the path by a constant value and, at each step, recomputing the local

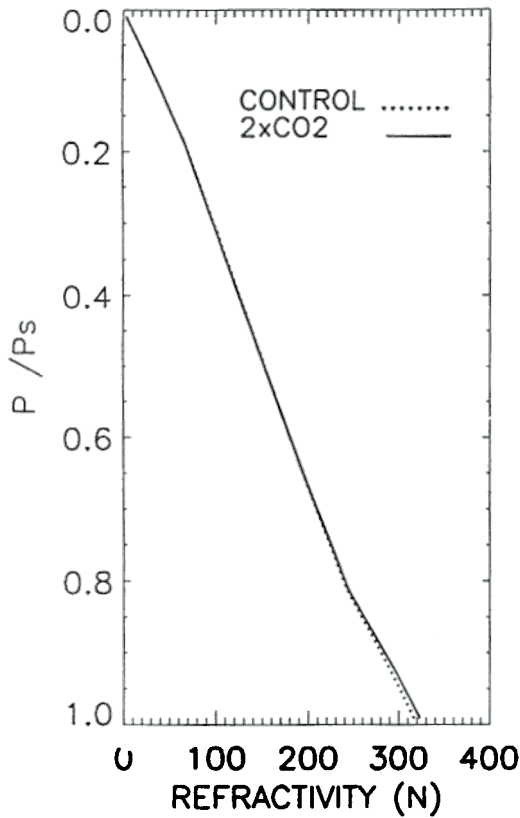


Fig. 11a. Globally averaged refractivity profiles for July, plotted versus sigma (P/P_s) vertical coordinates.

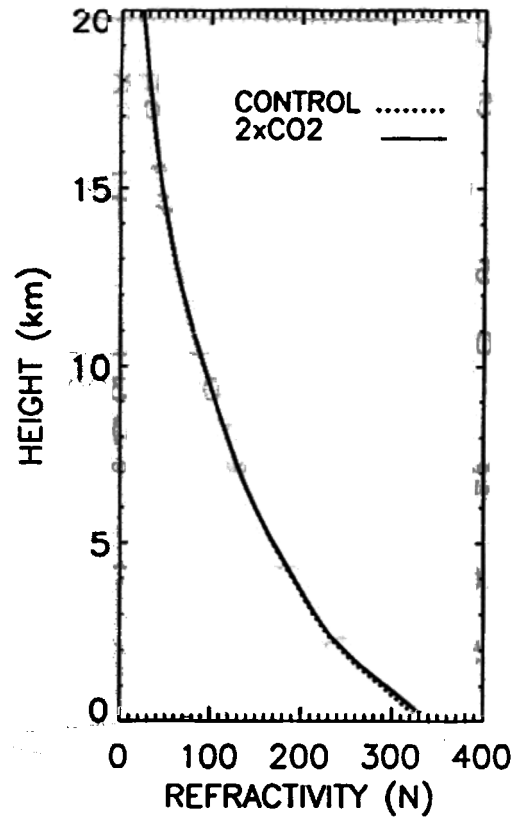


Fig. 12a. Globally averaged refractivity profiles for July, plotted versus altitude.

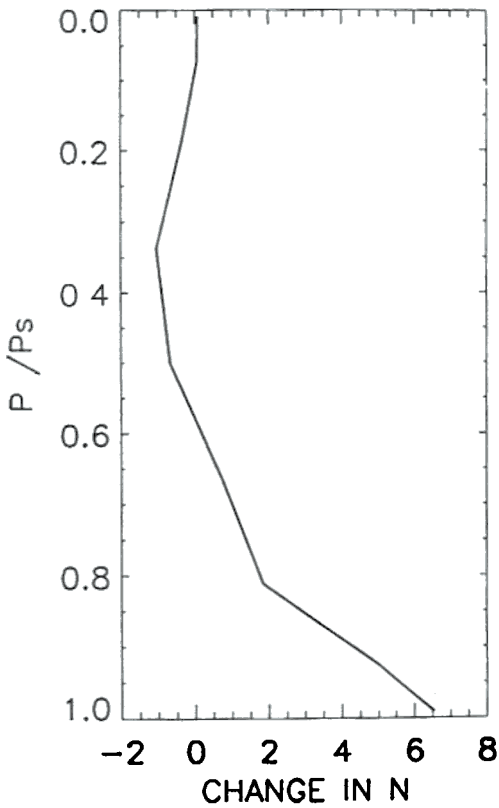


Fig. 11b. Differences in Figure 11a due to doubled CO_2 .

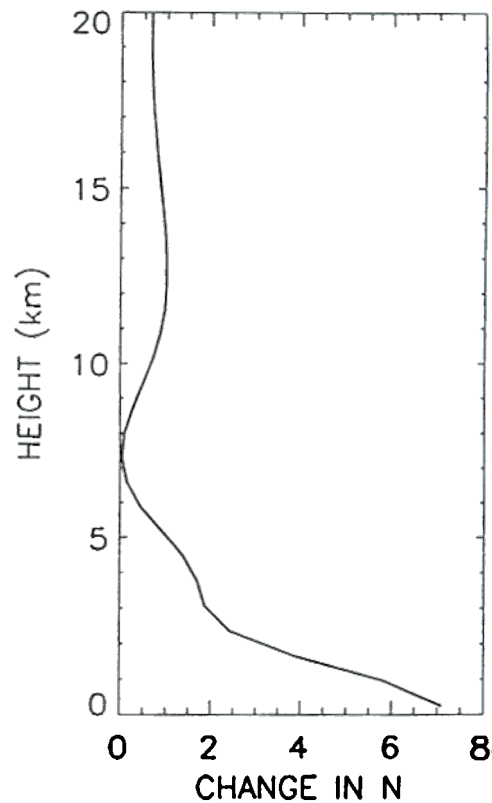


Fig. 12b. Differences in Figure 12a due to doubled CO_2 . Global average calculated only to 75° S due to topographic difficulties associated with the Antarctic continent.

refractivity and elevation angle. This process begins at a location corresponding to the minimum ray altitude (the height of the nearest approach of the GPS signal to the Earth) and is continued until the ray has exited the atmosphere, at which point, the exit location and elevation angle of the ray are recorded. Because of the assumed spherical symmetries of the atmosphere, the complete path could then be found by assuming an identical trace beginning at the same point and propagating in the opposite direction. From the exit location and angle of the signal values and the known altitudes of the two satellites, we compute the geometrical delay, using simple trigonometric relations. The total delay, then, is computed as the sum of the optical delay, which occurs while the signal travels through the atmosphere, and the geometrical delay, which results from the bending effect of the atmosphere. These total delays were computed for different values of the minimum ray altitude for control and $2\times\text{CO}_2$ cases. As can be seen in Figure 13, the bending component, or geometrical delay, grows as the ray approaches the surface of the Earth, eventually becoming the dominant factor. At the lowest level, the 1200 m of geometrical delay correspond to a total bending angle of approximately 1° .

Using the methods outlined above, occultation delays were calculated using globally averaged refractivity profiles in the simulated present and $2\times\text{CO}_2$ climates and plotted versus minimum ray altitude (Figure 14). A particularly strong warming signal of nearly 100 m occurs for occultation rays passing through the lower troposphere. This effect can be attributed to the increased water vapor content of the atmosphere. For rays which pass only through the upper atmosphere above 12 km in height, a consistent increase in delay can be detected (Figure 15). This change has a magnitude which ranges from approximately 1.0 to 1.5 m and can be attributed to the higher refractivities caused by increased total pressures. Thus in the upper regions of the atmosphere, where occultation measurements have the greatest

accuracy, the signal is small but detectable above the noise at these altitudes, and in the higher-error region of the lower atmosphere the signal is conveniently large.

Occultation delays for zonally averaged refractivities over various regions of the Earth were also calculated. Because the greatest atmospheric moisture increase occurs in the tropics, delays computed for zonally averaged refractivity profiles in this region produce a large warming signal, as much as 300 m, in the lower troposphere (Figure 16). When considered in light of the predicted error of 1 m, one sees that occultation delays in the tropics could be extremely sensitive indicators of global change.

In a doubled CO_2 climate the polar regions of the Earth exhibit an interesting contrast compared to the tropics and the global average. The south pole, in particular, exhibits a temperature increase of nearly 8 K between control and doubled CO_2 simulations. Because atmospheric water vapor content in this region is small in both simulations, the temperature increase is the dominant factor, and it causes a decrease in the local refractivity and a decrease in occultation delay of nearly 70 m at the surface (Figure 17). The reduced water vapor in this region would also provide for more accurate occultation data, making the potential of detection of this warming signal particularly promising. Overall, global and zonal averages of occultation delays appear to be quite sensitive to the simulated global warming, and when coupled with the ease and low cost (relative to other satellite sensing systems because of the modest weight and power requirements) with which these data can be obtained implies a formidable means of monitoring the Earth's atmosphere.

The strong "greenhouse warming" signature simulated here is due to the amplification of the atmospheric effects on the zenith GPS signal by the long "lever arms" of the LEO-atmosphere-GPS link, as indicated in Figure 18. A comparison of Figures 9 and 14 indicates that this amplification is about 3 orders of magnitude in

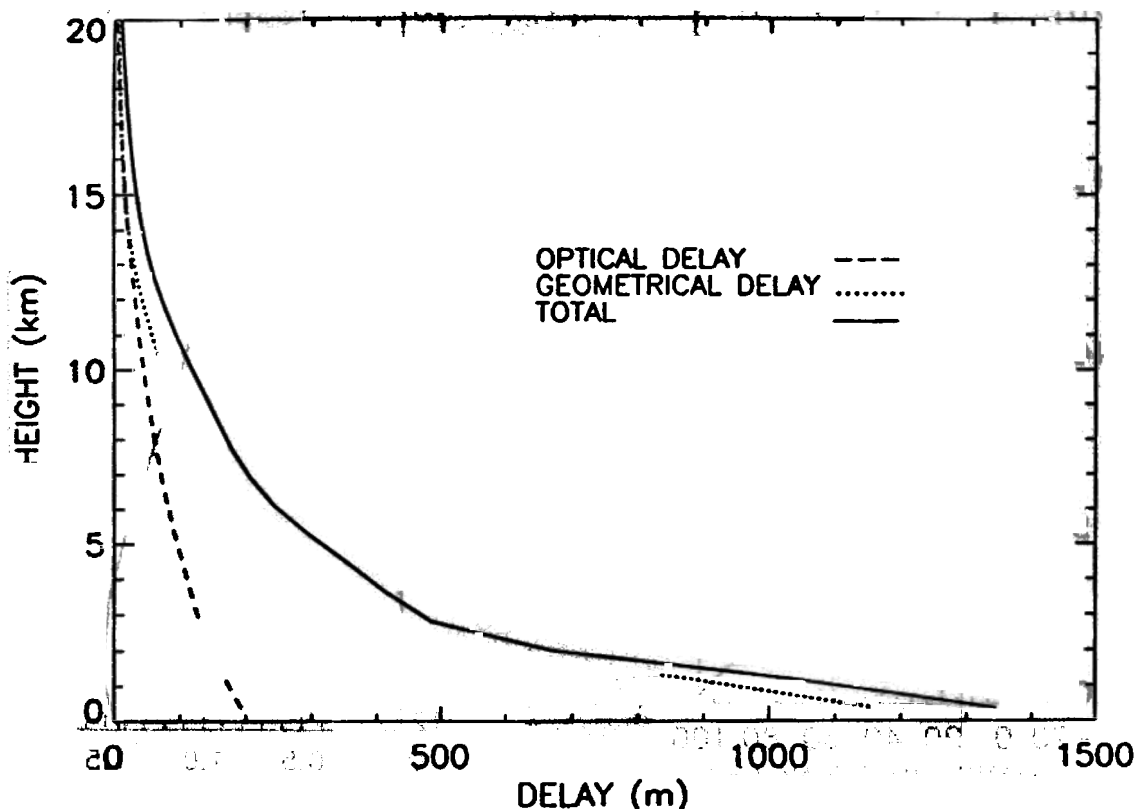


Fig. 13. Comparisons of relative contributions of geometrical and optical delay components in a simulated occultation measurement using globally averaged model data for July.

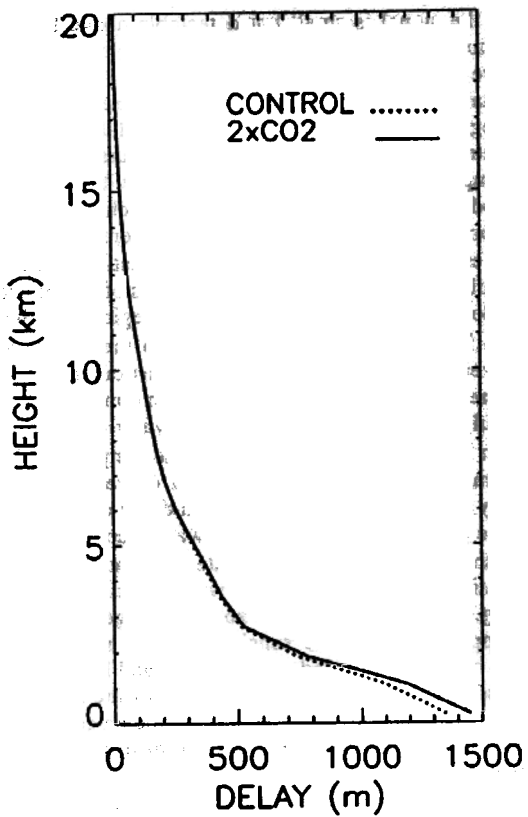


Fig. 14a. Occultation delays plotted versus the minimum altitude of ray for control and 2xCO₂ globally averaged data for July.

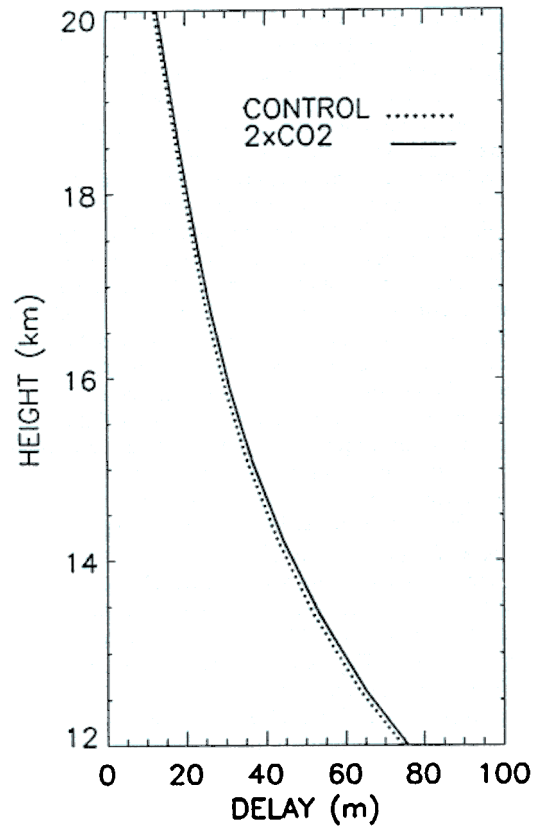


Fig. 15a. Detail of upper atmosphere occultation delay profiles in control and 2xCO₂ simulations.

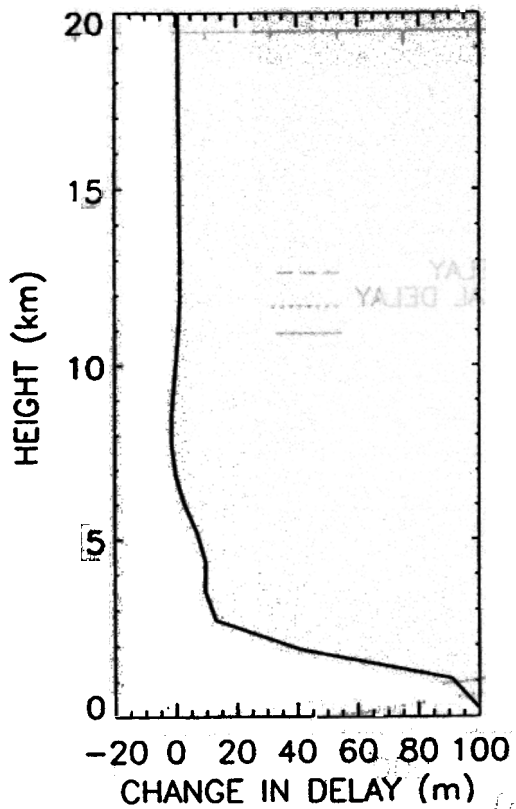


Fig. 14b. Differences in Figure 14a due to doubled CO₂. The southern polar cap has been excluded from the global average calculation, again, due to topographic difficulties.

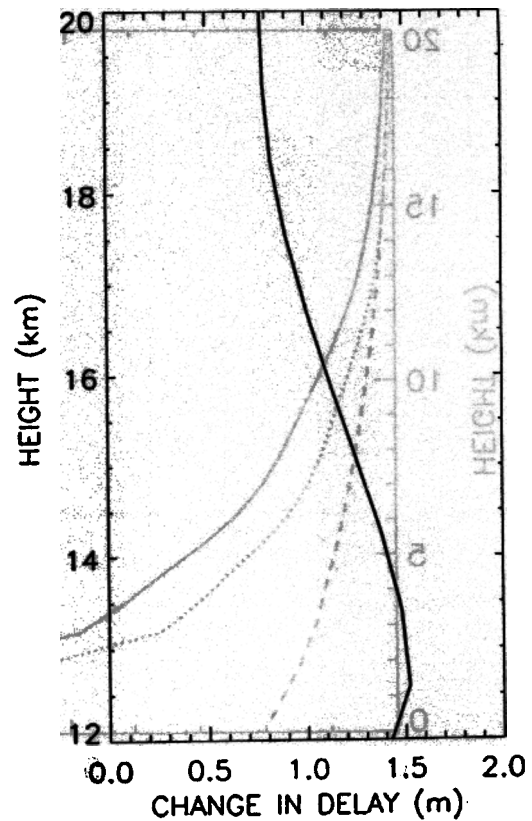


Fig. 15b. Differences in Figure 15a due to doubled CO₂.

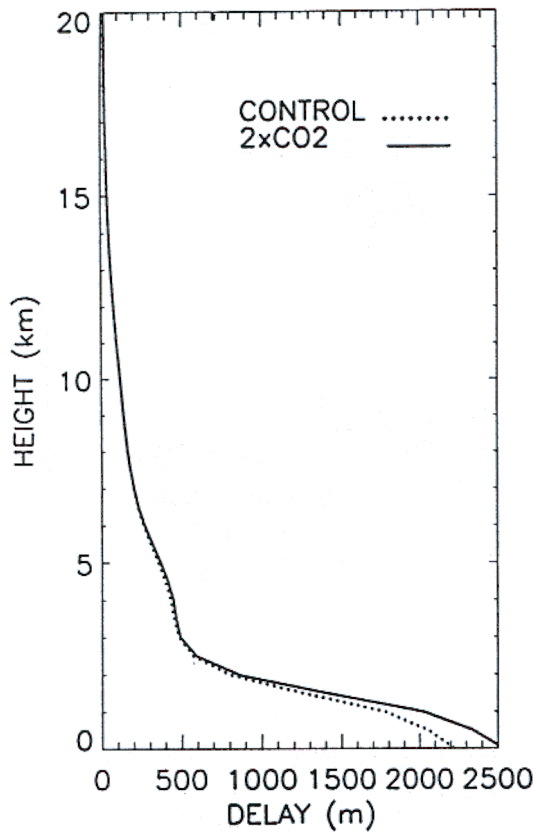


Fig. 16a. Occultation delay profiles for tropical zone (10°S - 10°N), averaged over July.

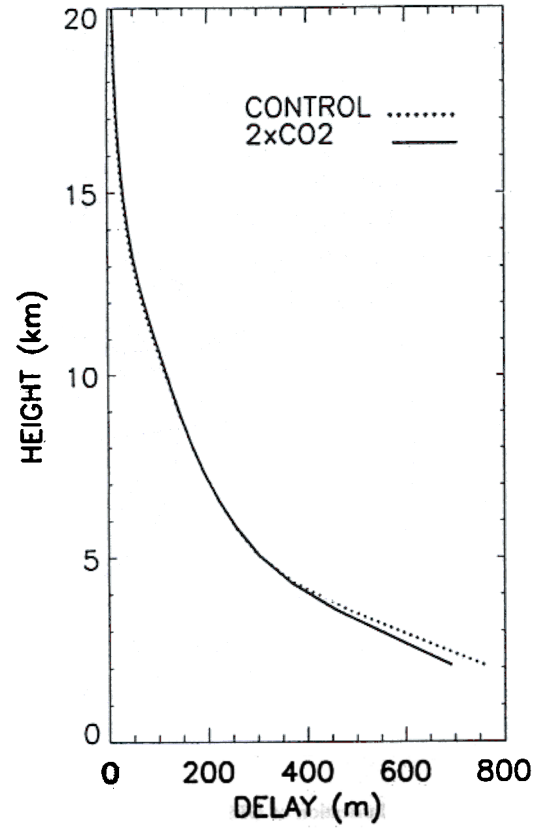


Fig. 17a. Occultation delay profiles for south polar zone (90°S - 78°S), averaged over July.

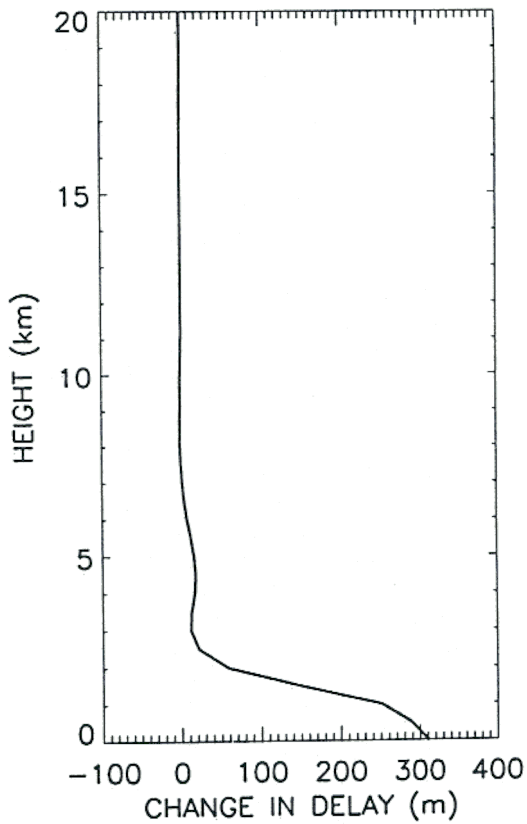


Fig 16b. Differences in Figure 16a due to doubled CO₂.

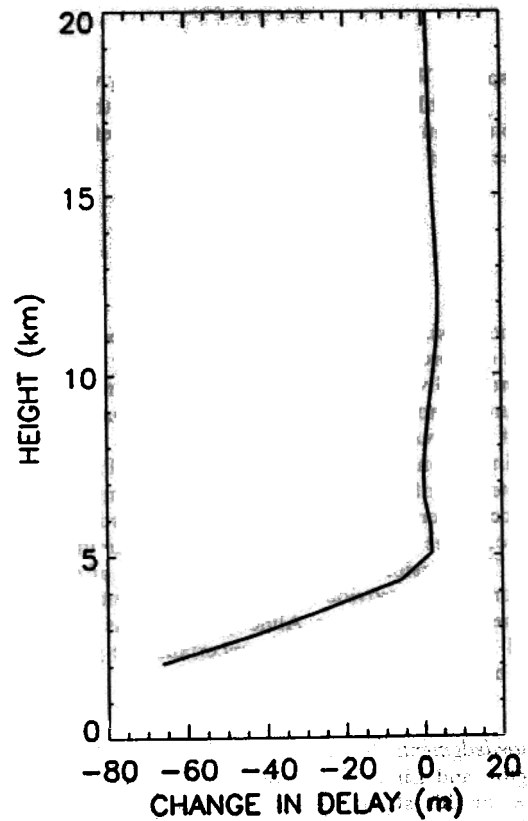


Fig. 17b. Differences in Figure 17a due to doubled CO₂.

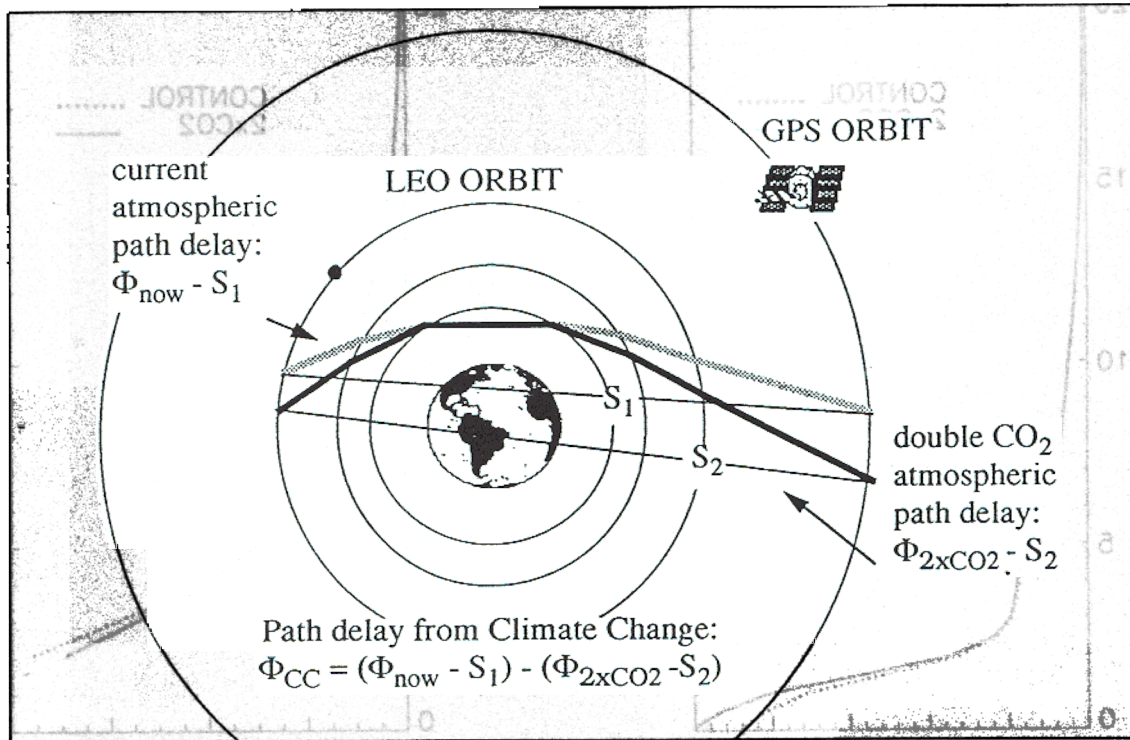


Fig. 18. Illustration of GPS occultation path delay resulting from climate change. Two rays that approach the Earth by a given minimum distance are shown. For each case the total path delay is the sum of (a) the integrated refractive delay along the bent ray path and (b) the geometric delay, defined as the difference in length of the refracted and line of sight paths. The large separation between the GPS and LEO satellites "amplifies" the geometric delay. We define the path delay from climate change as the difference in total path delay between the current and double CO₂ model atmospheres.

the troposphere. With this amplification, together with the global coverage possible with the LEO receivers, the GPS radio occultation technique has the potential for being effective for the early detection of climate change.

6. CONCLUSIONS

The model simulations described in this paper indicate that GPS data can provide useful precipitable water estimates with high accuracy. Given independent estimates of vertical profiles of temperature, it appears likely that useful estimates of vertical profiles of water vapor can be derived.

The simulations also show the potential of GPS meteorology for the detection of climate change. The fundamental observation of GPS occultations, the signal delay, exhibits distinct global and regional changes in response to the model-simulated global warming. The possibility for enormous numbers of global, daily observations would provide the means to constantly monitor the atmosphere for these changes. Although the details of the changes estimated by using the CCM are uncertain, the general trends appear to be reasonable.

Acknowledgments. We acknowledge the assistance of Warren Washington and Linda Verplank in making the NCAR CCM available for this study. This research was supported by the National Science Foundation through grants EAR91-16461 and EAR92-15533 and through its support to NCAR and UCAR..

REFERENCES

- Bevis, M., S. Businger, T. A. Herring, C. Rocken, R. A. Anthes, and R. H. Ware, *GPS meteorology: Remote sensing of atmospheric water vapor using the Global Positioning System*, *J. Geophys. Res.*, **97**, 15,787-15,801, 1992.
- Bevis, M., S. Businger, T. A. Herring, R. A. Anthes, C. Rocken, R. H. Ware, and S. Chiswell, *GPS meteorology: Mapping zenith wet delays onto precipitable water*, *J. Appl. Meteor.*, in press 1993.
- Brunner, F. K., and M. Gu, *An improved model for the dual frequency ionospheric correction of GPS observations*, *Manuscr. Geodet.*, **16**, 205-214, 1991.
- Elgered, G., J. L. Davis, T. A. Herring, and I. I. Shapiro, *Geodesy by radio interferometry: Water vapor radiometry for the estimation of wet delay*, *J. Geophys. Res.*, **96**, 6541-6555, 1990.
- Hardy, K. R., D. P. Hinson, G. L. Tyler, and E. R. Kursinski, *Atmospheric profiles from active space-based radio measurements*, paper presented at the Sixth Conference on Satellite Meteorology and Oceanography, American Meteorological Society, Atlanta, GA., January 5-10, 1992.
- Herring, T., J. L. Davis, and I. I. Shapiro, *Geodesy by radio interferometry: The application of Kalman filtering to very long baseline interferometry data*, *J. Geophys. Res.*, **95**, 12,561-12,581, 1990.
- Kuo, Y.-H., Y.-R. Guo, and E. R. Westwater, *Assimilation of precipitable water measurements into a mesoscale and numerical model*, *Mon. Weather Rev.*, **121**, 1215-1238, 1993.
- Meehl, G. A., and W. M. Washington, *CO₂ climate sensitivity and snow-sea-ice albedo parameterization in an atmospheric*

- GCM coupled to a mixed-layer ocean model*, *Clim. Change*, 16, 283-306, 1990.
- Smith, E. K., and S. Weintraub, *The constants in the equation for atmospheric refractive index at radio frequencies*, *Proc. IEEE*, 41, 1035-1037, 1953.
- Spilker, J. J., *Signal structure and performance characteristics*, *Global Positioning System, Navigation*, 1, 29-54, 1980.
- Washington, W. M., and G. A. Meehl, *Seasonal cycle experiment on the climate sensitivity due to a doubling of CO₂ with an atmospheric general circulation model coupled to a simple mixed-layer ocean model*, *J. Geophys. Res.*, 89, 9475-9503, 1984.
- Yunck, T. P., and W. G. Melbourne, *Geoscience from GPS tracking by earth satellites*, *JPL Geod. Geophys. Preprint 189*, 19 pp., December 1989.
- R. A. Anthes and W. D. Bonner, University Corporation for Atmospheric Research (UCAR), P.O. Box 3000, Boulder, CO 80307.
- M. G. Bevis and S. Businger, Department of Marine, Earth and Atmospheric Sciences, North Carolina State University, Raleigh, NC 27607.
- C. Rocken and R. H. Ware, University Navstar Consortium (UNAVCO), P.O. Box 3000, Boulder, CO 80307.
- L. L. Yuan, Stanford University, Stanford, CA 94305.

(Received November 9, 1992;
revised April 1, 1993;
accepted April 7, 1993.)